Large-eddy simulation of the supersonic cavity flow and its far field aero-acoustic characteristics

By B. Hu†, Z. Ren†, B. Wang† AND X. Y. Hu‡

† School of Aerospace, Tsinghua University, Beijing, China, 100084
‡ Lehrstuhl für Aerodynamik und Strömungsmechanik, Technische Universität München, Germany

The far field aero-acoustic characteristics of supersonic cavity flows was investigated by means of Large Eddy Simulation (LES) and acoustic analogy method. A fifth-order hybrid WENO compact scheme was used to calculate the convective flux, and sixth-order compact one for the viscous flux. The Farassat's Formula 1A was employed to solve the Ffowcs William-Hawkings (FW-H) equations to obtain the acoustic pressure fluctuations of far field. The effects of cavity configuration and flow Mach number on flow and aero-acoustic properties were analyzed. The ramp angle of rear-step determines the more-organized level of flow coherent structures and the wall static pressure decrease, which trend was available in the situation of low Mach number, compared with high Mach number flow. The main frequency is enhanced in the ramped rear-step cavity flow. The ramp has the function of aero-acoustic noise suppression, but the improvement is limited. The present conclusions are valuable for evaluating the performance of cavities embedded in supersonic flows in engineering applications.

1. Introduction

Cavities are widely used in both industrial and aerospace fields. For example, in a scramjet engine, cavity is applied as a flame holder to guarantee the success of ignition and reduce the ignition delay time under a wide range of operating conditions. The cavity increases the flow residence time and provides a perfect reaction zone, in which the flow velocity is relatively low comparing to the main flow. The flow over a weapon bay of a fighter plane can also be taken as cavity flows. The supersonic cavity flows cover important fundamental flow phenomena, such as the shedding of vortices, boundary layer separation, shear layer, linear/nonlinear acoustic waves, shock and expansion waves, and interactions between them.

From the late 1950s, people started to study cavity flows and carried out relevant experiments. Stallings [1] divided a supersonic cavity flow into three types according to the length-to-depth (L/D) ratio of cavity, which is open cavity $(L/D < 10)$, closed cavity $(L/D > 13)$ and transitional cavity $(L/D\tilde{}10 - 13)$. In an open cavity, the shear layer forms at the leading edge and attaches to the rear wall of the cavity. Weak shock waves exist at the separation and reattachment point, inducing high intensity acoustic waves. A closed cavity refers to the shear layer not covering the whole cavity but attaching to the bottom wall of the cavity. Two recirculation zones are formed and no acoustic waves

appear. The flow in a transitional cavity is in the intermediate state between the open and closed cavity.

Tracy and Plenovich [2,3] conducted experiments to study the subsonic and transonic flows over cavities with different L/D ratios. They found that the open and transitional-open cavity flows support the tone generation for the subsonic flow as the Mach number is greater than 0.6 and the cavity changes from the resonant to non-resonant one as the L/D increases. Murray and Elliot [4] found that the two dimensionality of the supersonic cavity flow decreases with an increasing Mach number. Zhang et al. [5] numerically simulated compressible flows over cavities with different L/D using different eddy-viscosity turbulence models. Ukeiley and Murray [6–8] pointed out that the scale of vorticity with respect to aft wall determined whether the resonance happened in the subsonic cavity or not. The above studies focused on the flow features with varying geometries in a wide range of Mach number. With the development of computational technology as well as turbulent models, more and more numerical simulations were performed to show the refined flow structures and analyze the physical mechanism. However, investigations on flow oscillations and aero-acoustics are not well enough.

Rossiter [9] revealed the oscillation mechanism coupling vortex shedding and acoustic modes, and first proposed a semi-empirical formula to predict the main frequencies of flow-acoustic oscillations in cavity, named as 'Rossiter mode'. Then, Heller and Bliss [10] corrected the Rossiter's formula for higher speed according to their experimental and analytical studies. Bilanin et al. [11] raised another analytical model to predict the aero-acoustic modes. The above analytical models work well under some certain conditions, but none of them is universal.

Kaufman and Clark [12] measured the flow field and aero-acoustic environment of cavity at subsonic and supersonic flow conditions. They found that the Sound Pressure Level (SPL) increases with the flow Reynolds number increasing, but the modal peaks do not change. Rockwell et al. [13, 14] showed that the separation from the leading corner of the cavity dominate the cavity flow. Zhang [15] proposed that the flow oscillation and wave emission are directly caused by the shear layer deflection. Rowley et al. [16, 17] applied a two-dimensional Direct Numerical Simulation (DNS) to study the modes of oscillation and acoustic fields radiated by compressible flows over open cavities, indicating a transition from a shear-layer mode, for the shorter cavities and lower Mach numbers, to a 'wake mode', for the longer cavities and higher Mach numbers. Bogey and Bailly [18], Hamed et al. [19], and Kerschen et al. [20] discussed the computational methods used in the three-dimensional acoustic simulation of cavity flow. Lai and Luo [21] proposed a three-dimensional hybrid LES-acoustic analogy method for predicting the noise of a subsonic open cavity. Thaker et al. [22] found the amplitudes of pressure oscillations corresponding to shock oscillations are higher than those of the acoustic pressure inside the cavity. But, the dominant factors of determining the pressure oscillation amplitudes are still unclear. Besides, the mechanisms of suppressing the pressure fluctuation and aero-acoustic noise of a cavity were also explored by using porous floors and slot vents [23], leading edge oscillating flaps [24], zero-net mass injection [25] and active actuators [26,27].

The literature reviews showed that amount of researchers focused on the studies of subsonic cavity flows and revealed their acoustic characteristics, while few studies of supersonic cases were conducted to analyze the physical mechanisms, which are more complicated. Therefore, the flow and aero-acoustic characteristics of supersonic cavity flows will be investigated by means of an LES-acoustic analogy method. First, the

means of LES coupling the immersed boundary method for calculating the supersonic turbulent cavity flow and aero-acoustic analogy for calculating the aero-acoustic pressure are introduced, respectively. Then, the coherent flow structures in a supersonic cavity are analyzed in details. Finally, frequency spectrum analysis of the aero-acoustic pressure of far field and the SPL distributions are discussed. The acoustic analogy theory used in the present paper is the *Farassat's formula 1A* based on the *Ffowcs William-Hawkings (FW-H) equation*.

2. Numerical method

2.0.1. *Large Eddy Simulation*

The unsteady compressible LES equations for mass, momentum, total energy, neglecting the body force and external heat source read as,

$$\frac{\partial \bar{\rho}}{\partial t} + \frac{\partial \bar{\rho}\tilde{u}_j}{\partial x_j} = 0 \tag{2.1}$$

$$\frac{\partial \bar{\rho}\tilde{u}_i}{\partial t} + \frac{\partial \left(\bar{\rho}\tilde{u}_i\tilde{u}_j + \bar{p}\delta_{ij} - \bar{\tau}_{ij} + \tau_{ij}^{sgs}\right)}{\partial x_j} = 0 \tag{2.2}$$

$$\frac{\partial \bar{\rho}\tilde{E}}{\partial t} + \frac{\partial \left[\left(\bar{\rho}\tilde{E} + \bar{P}\right)\tilde{u}_j - \bar{u}_i\bar{\tau}_{ij} + \bar{q}_j + q_j^{sgs}\right]}{\partial x_j} = 0 \tag{2.3}$$

where '–' represents large eddy simulation filter and '~' for the Favre-filtered one. The perfect gas equation of state is used to close the above equations,

$$P = \bar{\rho}\tilde{R}\tilde{T} \tag{2.4}$$

The subgrid-scale terms are denoted with the *sgs* superscript, such as the subgrid stress $\tau_{ij}^{sgs}$and subgrid diffusion of energy q_j^{sgs},

$$\tau_{ij}^{sgs} = \left(\bar{u}_i\bar{u}_j - \bar{\bar{u}}_i\bar{\bar{u}}_j\right) = 2\left(C_S\Delta\right)^2\bar{S}_{ij}\left(2\bar{S}_{ij}\bar{S}_{ij}\right)^2 - \frac{1}{3}\bar{\tau}_{kk}\delta_{ij} \tag{2.5}$$

$$q_j^{sgs} = -\frac{C_s\tilde{\rho}\Delta^2\sqrt{2\bar{S}_{ij}\bar{S}_{ij}}}{\mathrm{Pr}}\frac{\partial\bar{T}}{\partial x_j} \tag{2.6}$$

Δ is the local grid size and set as the cubic root of the cell volume, $\Delta = \sqrt[3]{\Delta x\Delta y\Delta z}$.

A finite difference methodology is used to solve the above governing equations. An explicit Runge-Kutta time-integration methodology is applied, obtaining a third-order time-accurate computation. The non-viscous fluxes $\hat{f}_{j+\frac{1}{2}}$, for the interface at $j + 1/2$, are evaluated using a fifth-order hybrid compact-WENO scheme [28] for the resolution of turbulent fields and shock-capturing calculation in the supersonic flows. A sixth-order symmetric compact difference scheme is applied for the viscous diffusion terms.

A schematic of the computational domain is shown in Figure 1. The inlet is the supersonic inflow. The top boundary is set as infinity and do not affect the internal flow. The bottom boundary is the non-slip wall to simulate the real boundary condition. An immersed boundary method [29] is used to construct the cavity configuration, as shown in shadow areas in Fig. 1.

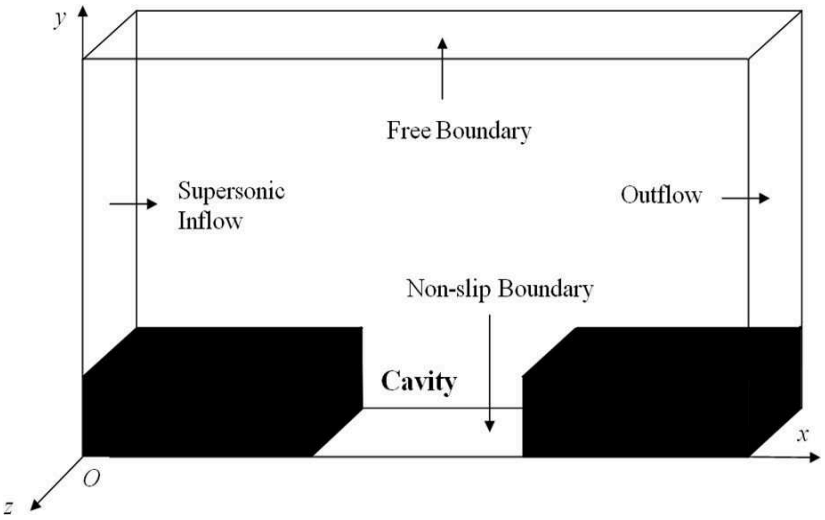

FIGURE 1. Schematic of computational domain and boundary conditions.

Length-to-depth ratio	Mach number	Stagnation temperature (K)	Stagnation pressure (kPa)
L/D	Ma	T_0	P_0
3	3	300	690

TABLE 1. Calculation parameters for validation case.

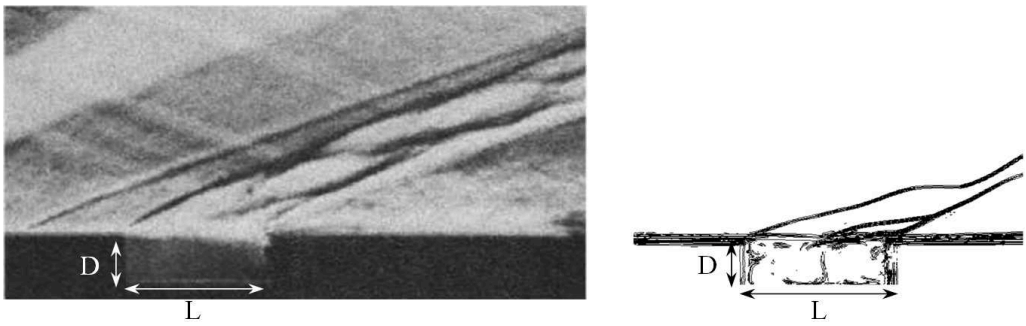

FIGURE 2. Schlieren photograph of cavity fields (left: Gruber's experiment results, right: present results).

2.0.2. *Validation of LES procedures*

The validation of the numerical method was carried out first, comparing with the experiment study of supersonic cavity flows conducted by Gruber et al. [30]. The calculation parameters were shown in Table 1.

Figure 2 shows the comparisons of flow fields by presenting the schlieren photograph of the experiment and present simulation. Two compression waves are formed at the leading edge and trailing edge of cavity, separately, which are similar with the experiment results.

Figure 3 presents the wall static pressure distribution along the cavity wall. Kim's LES result [31] is included in the comparison. In this figure, the effective distance is repre-

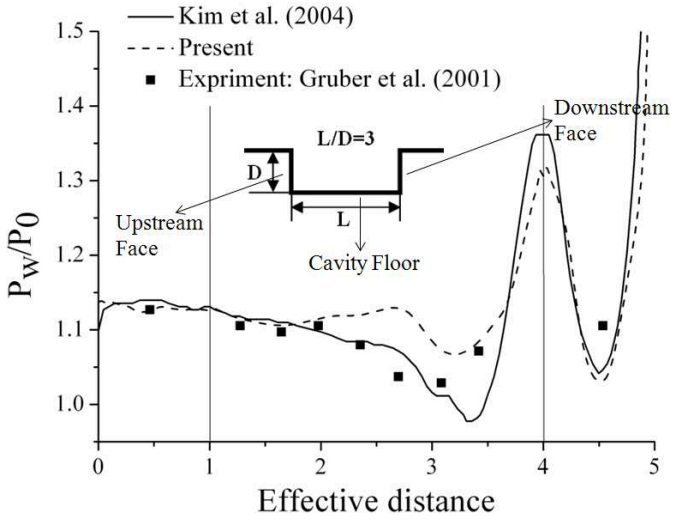

FIGURE 3. Time-averaged wall static pressure distributions.

sented by three segments: the cavity upstream face from the leading edge, the cavity floor and the cavity rear face. The present numerical result agrees well with Gruber's experiment, better than Kim's LES result at some observation points.

2.0.3. *Acoustics analogy*

The acoustic analogy scheme is based on the FW-H equation which was derived by Ffowcs Williams and Hawkings [32]. The Farassat's Formulation 1A, developed by Farassat [33] in 1983, was the most widely used solution of the above form of FW-H equation, which is used in the present simulation of acoustics analogy.

2.0.4. *Verification of the aero-acoustic analogy*

Generally, it is hard to validate the acoustic analogy for a complex flow, because there is no analytical solution in most cases. Therefore, a monopole case, of which analytical solution is available, is used here to verify the analogy calculation. For a single-frequency monopole, the complex potential is calculated as,

$$\phi = \frac{1}{4\pi}\left[\frac{A\cos(\omega t)}{r(1-M_r)}\right]_{\tau=t-\frac{r}{a}} \tag{2.7}$$

Then the pressure, velocity and density field of a still monopole can be obtained by,

$$p' = \frac{\partial\phi}{\partial t} = -\frac{A\omega}{4\pi r}\sin\left(t-\frac{r}{a}\right) \tag{2.8}$$

$$\rho' = \frac{1}{a^2}\frac{\partial\phi}{\partial t} \tag{2.9}$$

$$u_i = -\frac{1}{\rho_0}\frac{\partial\phi}{\partial x_i} = \frac{A}{4\pi r^2\rho_0}\left[-\frac{\cos\left(t-\frac{r}{a}\right)}{r}+\frac{\omega}{a}\sin\left(t-\frac{r}{a}\right)\right] \tag{2.10}$$

The integral surface is taken as $f = \sqrt{x^2+y^2+z^2} - r_1 = 0$. $N \times N$ panels (integral

Parameter	Value
A	1
ω	$20\pi[rad/s]$
M (Mach number of monopole)	0.0
ρ_0	$0.611[kg/m3]$
a	$207.485[m/s]$
Position of monopole	$(0,0,0)[m]$
Position of observer	$(100,0,0)[m]$
r_1	$3.0, 10.0[m]$
N	$10, 40$

TABLE 2. Parameter values used in the monopole case.

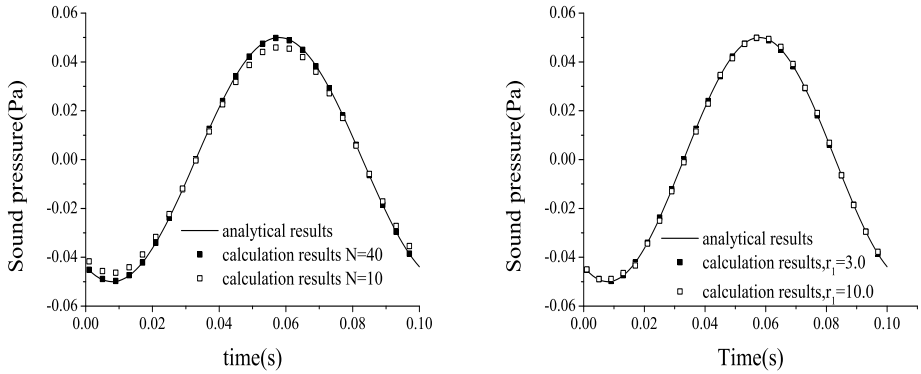

(a) different panel number (r1=3; N=10 or 40) (b) different integral surface position (r1=3 or 10; N=40)

FIGURE 4. Comparison between analytical results and calculation results.

elements) are divided on the integral surface. The parameter values are shown in Table 2.

As shown in Fig.4(a), if the integral surface is taken as $r_1 = 3.0$ and the panel numbers are 40×40, the calculated acoustic pressures agree perfectly well with the analytical results and the errors are less than 2%. But when the panel numbers changed to 10×10, there will be big errors between the calculated and analytical results. Therefore, adequate panels are needed to guarantee the essential accuracy of acoustic calculation.

According to the comparison in Fig.4(b), the analytical and the calculation results with different integral surfaces position agree well. If all sources are covered inside the integral surface, the position of integral surface ($r_1 = 3.0$ or 10.0) is no longer important for calculation of the acoustic pressure. But a bigger integral surface may need more panels, and it may be quite expensive and inefficient sometimes.

3. Results and discussion

Based on the validation of LES, simulations are conducted for three different cases, which consider the influence of inlet parameters and the configurations of cavities. Three observers are placed above the cavity. Observer 2 locates at ($x = 0.0582m, y = 1.0m, z =$

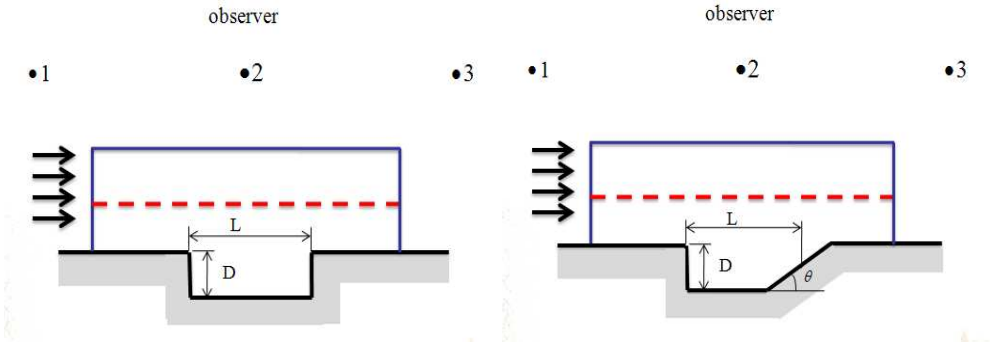

(a) Geometry configuration and observer position for Case 1: standard rectangle cavity.

(b) Geometry configuration and observer position for Case 2: rectangle cavity with ramp.

FIGURE 5. Sketch of computation configuration.

Case No	L/D	Ramp angle (deg) θ	Mach number Ma	Pressure (kPa) P	Temperature (K) T
1	3.88	90	1.75	100	820
2	3.88	30	1.75	100	820

TABLE 3. Cavity geometry specifications and inlet parameters.

$0.0m$). The horizontal distance between observer 1 and observer 2 (or between observer 2 and observer 3) is $1.0m$.

Figure 5 shows the geometrical configuration of Case 1 and Case 2. Table 3 shows the geometric features of cavities and inlet flow conditions. Both cases have the same depth, $D = 10mm$. The length L of cavity with ramp rear-step is defined as the distance from the leading edge to the middle of the ramp. θ is the ramp angle.

3.1. *Flow characteristics*

Figure 6 shows the distributions of normalized wall static pressure for Case 1 and Case 2. The results are plotted as the function of distance, which is defined in Section 2.1.4. A compression wave forms at the leading edge, resulting in a light rising of pressure, which is similar with those in Fig. 3. The pressure diminishes along the bottom wall, and then increase to peak at the corner near the cavity floor due to the recompression of cavity shear layer at the aft wall, forming a stagnation point. After the corner, the fluid inside the cavity interacts with the aft wall periodically, resulting in pressure decreasing at first, and then increasing. If the ramp angle changes to 30 deg, the pressure distribution seems similar with that of Case 1, though distributes at a more reduced level. However, under the influence of ramp, pressure appears rising weakly at the aft wall corner.

Figure 7 shows a clearer illustration of flow field in the cavity. The flow structures in the rectangle cavity geometry are noticeably different from the cavity with aft wall angle geometry. The rectangle cavity showed three large rotating vortexes, however, the cavity with ramp comprises a primary vortex and several smaller secondary vortexes near upstream face and cavity floor. With the introduction of ramp, the impact of vortexes on the aft wall is not as intense as that of rectangle cavity and the feedback effects of

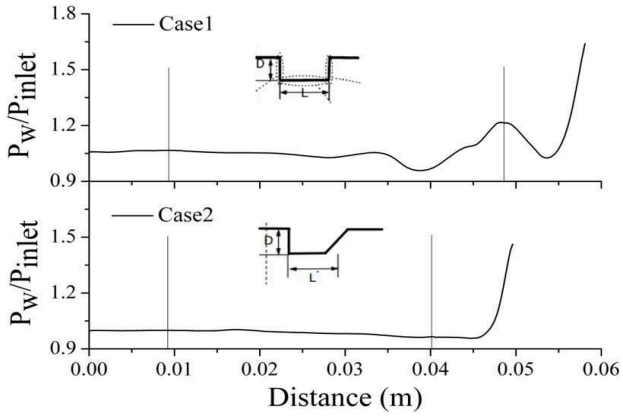

FIGURE 6. Time-averaged wall static pressure distributions. (up: Case 1, down: Case 2)

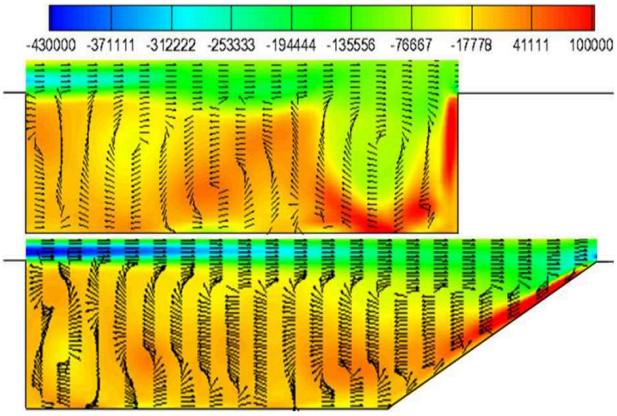

FIGURE 7. Time-averaged vorticity contours in cavities. (up: Case 1, down: Case 2)

eddies are weaker. Hence, the distribution of wall static pressure is smoother and flow structures inside the cavity are more organized for Case 2.

3.1.1. *Aero-acoustic characteristics*

With the data of flow field calculated above, the acoustic analogy is applied to calculate the acoustic characteristics of observer position in the far field. As shown in Fig. 5, the calculation domain in LES is circled by solid lines in Case 1 and Case 2, and the dash lines represent the upper boundary of integral surface, which is similar with Luo's treatments [21]. The region circled by the dash line and contour line of cavity is the region of acoustic sources. We adjust the position of dash line until the results of acoustic calculation are basically unchanged, which guarantees that all the sources are included in the integral surface.

Figure 8 provides the sound pressure changing with time at different observer positions. For each observer, the pressure oscillations appear to be periodic, but are not strict because of the different peak values at different cycles. The waveforms of each cycle are similar.

The acoustic pressure magnitudes of the same observer are similar for Case 1 and Case 2. Comparing with observers 1 and 3, sound pressures of observer 2 are higher.

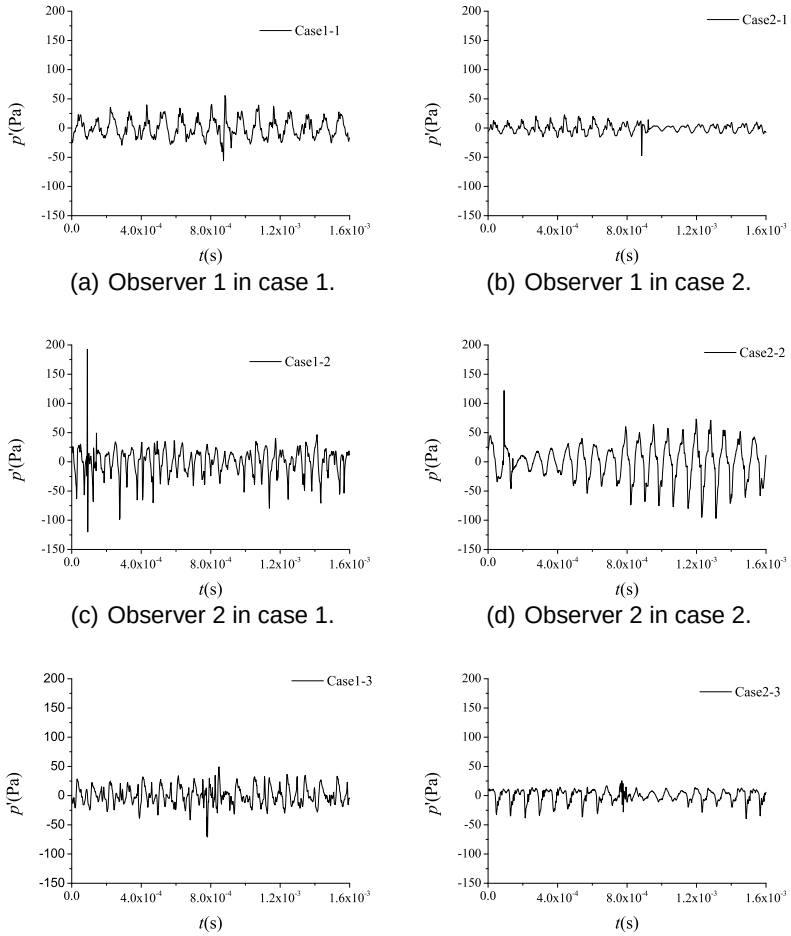

(a) Observer 1 in case 1. (b) Observer 1 in case 2.

(c) Observer 2 in case 1. (d) Observer 2 in case 2.

(e) Observer 3 in case 1. (f) Observer 3 in case 1.

FIGURE 8. Sound pressure-time curves.

Relatively, the waveforms of sound pressure in Case 2 are clearer than that in Case 1, which may imply the different frequency distribution of the two cases.

Figure 9 shows the comparison of frequency spectrum of acoustic pressure at observer 1. For Case 1, there are three acoustic modes in the low-frequency regions, which is $(1), (2), (3),$ respectively. While for Case 2 in the low-frequency regions, only one acoustic modes–(4)– can be clearly identified. Also, the acoustic mode (4) of Case 2 is of much lower magnitude than that of Case 1. For high-frequency regions, the magnitudes of frequency for Case 2 are generally lower comparing to the magnitudes for Case 1.The energy of the pressure oscillation concentrates on the high frequency parts. Thus, the acoustic energy of Case 1 will be higher and the acoustic noise generation is more intense. It can be concluded that the ramp is effective on suppressing the aero-acoustic noise of cavity flow.

Figure 10 shows the contour of SPL. The SPL of far-field is calculated as below,

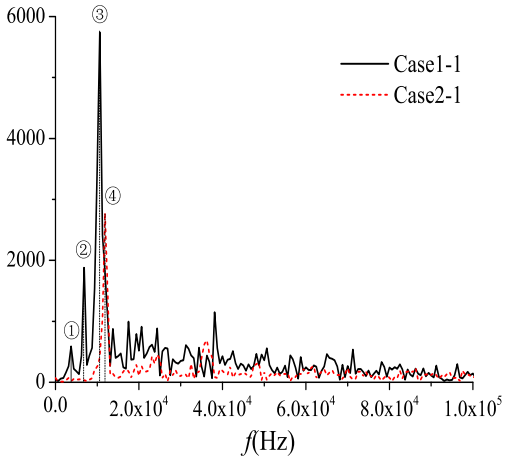

FIGURE 9. Comparison of frequency spectrum of acoustic pressure at observer 1.

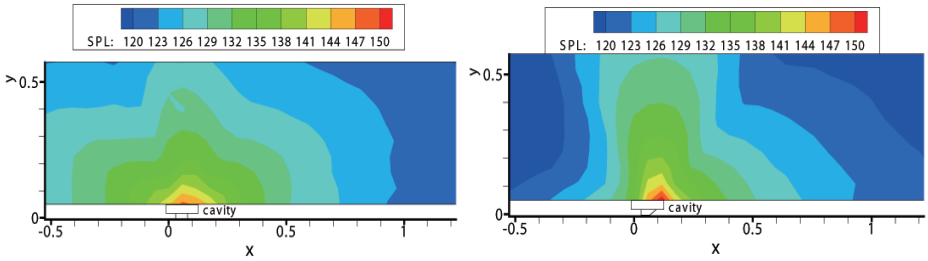

(a) case 1. (b) case 2.

FIGURE 10. Contour of SPL.

$$SPL = 20\log_{10}\left(\frac{p'_{rms}}{2\times10^{-5}}\right) \tag{3.1}$$

There is a banded distribution of SPL in the far field. The SPL becomes higher with the decrease of distance between the observer and the acoustic sources in the cavity. The acoustic noises generated by the supersonic cavity flow mainly concentrate on the region above the cavity.

4. Conclusions

With the LES and a subsequent acoustic analogy, a study on the flow features and acoustic characteristics of supersonic cavity flows were conducted. The validation case of Gruber's experiment and the acoustic calculation of a still monopole showed the reliability of the present numerical methods, respectively.

It was found that the ramp angle of trailing edge influenced the characteristics of cavity flow significantly, including the organized level of coherent flow structures and distributions of wall static pressure. Flow structures inside the cavity with a ramp yielded more organized and the wall pressure decreased. The magnitudes of acoustic modes

and SPL values of the cavity with ramp are generally lower than those of the standard rectangle cavity. Ramps of trailing edge do have effects on suppression of pressure fluctuation and acoustic noise, but the SPL contour shows that the improvements are relatively limited.

References

[1] STALLINGS, R. L. AND WILCOX, F. J. (1987). Experimental cavity pressure distributions at supersonic speeds.*NASA Technical Paper 2683*.

[2] TRACY, M. B. AND PLENTOVICH, E. B. (1993). Characterization of cavity flow fields using pressure data obtained in the Langley 0.3-meter transonic cryogenic tunnel. *NASA Technical Memorandum 4436*.

[3] TRACY, M. B. AND PLENTOVICH, E. B. (1997). Cavity unsteady-pressure measurements at subsonic and transonic speeds. *NASA Technical Paper 3669*.

[4] MURRAY, R. C. AND ELLIOTT,G. S. (2001). Characteristics of the compressible shear layer over a cavity. *AIAA Journal*, **39**(5), 846–856.

[5] ZHANG, J., MORISHITA, E., OKUNUKI, T. AND ITOH, H. (2001). Experimental and computational investigation of supersonic cavity flows. *AIAA Paper 2001-1755*.

[6] UKEILEY, L. AND MURRAY, N. (2005). Velocity and surface pressure measurements in an open cavity. *Experiments in Fluids*, **38**, 656–671.

[7] MURRAY, N. AND UKEILEY, L. (2003). Estimation of the flow field from surface pressure measurements in an open cavity. *AIAA Journal*, **41**(5), 969–972.

[8] MURRAY, N. AND UKEILEY, L. (2007). Modified quadratic stochastic estimation of resonating subsonic cavity flow. *Journal of Turbulence*, **53**(8).

[9] ROSSITER, J. E. (1964). Wind tunnel experiments of the flow over rectangular cavities at subsonic and transonic speeds. *ARC R. & M.*, **3458**.

[10] HELLER, H. AND BLISS, D. (1975). The physical mechanisms of flow-induced pressure fluctuations in cavities and concepts for their suppression. *AIAA Paper 1975-0491*.

[11] BILANIN, A. J. AND COVERT, E. E. (1973). Estimation of possible excitation frequencies for shallow rectangular cavities. *AIAA Journal*, **11**(3), 347–351.

[12] KAUFMAN, L. G., MACIULAITIS, A. AND CLARK R. L. (1983). Mach 0.6 to 3.0 flows over rectangular cavities. *ATWAL-TR-82-3112*, U. S. Air Force.

[13] ROCKWELL, D. AND KNISELY, C. (1979). The organized nature of flow impingement on a corner. *Journal of Fluid Mechanics*, **93**(3), 413–432.

[14] LIN, J. C. AND ROCKWELL, D. (2001). Organized oscillations of initially turbulent flow past a cavity. *AIAA Journal*, **39**(6), 1139–1151.

[15] ZHANG, X. (1995). Compressible cavity flow oscillation due to shear layer instabilities and pressure feedback. *AIAA Journal*, **393**(8), 1404–1411.

[16] ROWLEY, C. W., COLONIUS, T. AND BASU, A. J. (2002). On self-sustained oscillations in two-dimensional compressible flow over rectangular cavities. *Journal of Fluid Mechanics*, **455**, 315–346.

[17] COLONIUS, T., BASU, A. J. AND ROWLEY, C. W. (1999). Computation of sound generation and flow/acoustic instability in the flow past an open cavity. *Proceedings of FEDSM99 3rd ASME/JSME Joint Fluids Engineering Conference, FEDSM99-7228*.

[18] BOEGY, C. AND BAILY, C. (2002). Three-dimensional non-reflective boundary conditions for acoustic simulations: far field formulation and validation test cases.

Acta Acoustics, **88**, 463–471.

[19] HAMED, A., BASU, D. AND DAS, K. (2003). Detached eddy simulations of supersonic flow over cavity. *AIAA Paper 2003-549*.

[20] ALVAREZ, J. O., KERSCHEN, E. J. AND TUMIN, A. (2004). A theoretical model for cavity acoustic resonances in subsonic flow. *AIAA Paper 2004-2845*.

[21] LAI, H. X. AND LUO, K. H. (2007). A three-dimensional hybrid LES-acoustic analogy method for predicting open-cavity noise. *Flow Turbulence Combust.*, **79**, 55–82.

[22] THAKERA, I. H. AND SOMANDEPALLI, V. S. R. (1999). Characterization of acoustic field induced by flow past cavities in supersonic combustors. *AIAA Paper 1999-2367*.

[23] STALLING, R. L., PLENTOVICH, E. B. AND TRACY, M. B. (1994). Effect of passive venting on static pressure distributions in cavities at subsonic and transonic speeds. *NASA Technical Memorandum 4549*.

[24] SHAW, L. (1998). Active control for cavity acoustic. *AIAA Paper 1998-2347*.

[25] ROWLEY, C. W. AND WILLIAMS, D.R. (2003). Control of forced and self-sustained oscillations in the flow past a cavity. *AIAA Paper 2003-0008*.

[26] YAN, P., DEBIASI, M. AND YUAN, X. (2004). Controller design for active closed-loop control of cavity flow. *AIAA Paper 2004-0573*.

[27] YAN, P., DEBIASI, M. AND YUAN, X. (2006). Experimental study of linear closed-loop control of subsonic cavity flow. *AIAA Journal*, **44**(5), 929–938.

[28] REN, Y. X., LIU, M. AND ZHANG, H. X. (2003). A characteristic-wise hybrid compact-WENO scheme for solving hypersonic conservation laws. *Journal of Computational Physics*, **192**, 365–386.

[29] PESKIN, C. S. (1972). Flow patterns around feat valves: a numerical method. *Journal of Computational Physics*, **10**, 252–271.

[30] GRUBER, C. S., BAURLE, R. A. AND MATHUR, T. (2001). Fundamental studies of cavity-based flameholder concepts for supersonic combustor. *Journal of Propulsion and Power*, **17**(1), 146–153.

[31] KIM, K. M., BAEK, S. W. AND HAN, C. Y. (2004). Numerical study on supersonic combustion with cavity-based fuel injection. *International Journal of Heat and Mass Transfer*, **47**, 271–286.

[32] FFOWCS WILLIAMS, J. E. AND HAWKINGS, D. L. (1969). Sound generated by turbulence and surfaces in arbitrary motion. *Philosophical Transactions of the Royal Society A*, **264**(1151), 321–342.

[33] FARASSAT, F. AND SUCCI, G. P. (1980). A review of propeller discrete frequency noise prediction technology with emphasis on two current methods for time domain calculations. *Journal of Sound and Vibration*, **71**(3), 399–419.